

# Behavior of Saline Ice under Cyclic Flexural Loading

Andrii Murdza<sup>1</sup>, Erland M. Schulson<sup>1</sup>, Carl E. Renshaw<sup>1,2</sup>

<sup>1</sup>Thayer School of Engineering, Dartmouth College, Hanover, NH, USA, 03755

<sup>2</sup>Department of Earth Sciences, Dartmouth College, Hanover, NH, USA, 03755

*Correspondence to:* Andrii Murdza (Andrii.Murdza@dartmouth.edu)

**Abstract.** New systematic experiments reveal that the flexural strength of saline S2 columnar-grained ice loaded normal to the columns can be increased upon cyclic loading by about a factor of 1.5. The experiments were conducted using reversed cyclic loading over ranges of frequencies from 0.1 to 0.6 Hz and at a temperature of -10 °C on saline ice of two salinities:  $3.0\pm 0.9$  and  $5.9\pm 0.6$  ‰. Acoustic emission hit rate during cycling increases with an increase of stress amplitude of cycling. Flexural strength of saline ice of  $3.0\pm 0.9$  ‰ salinity appears to increase linearly with increasing stress amplitude, similar to the behavior of laboratory-grown freshwater ice (Murdza et al., 2020b) and to the behavior of lake ice (Murdza et al., 2021). The flexural strength of saline ice of  $5.9\pm 0.6$  ‰ depends on the vertical location of the sample within the thickness of an ice puck; i.e., the strength of the upper layers, which have a lower brine content, was found to be as high as three times that of lower layers. The fatigue life of saline ice is erratic. Cyclic strengthening is attributed to the development of an internal back stress that opposes the applied stress and originates possibly from dislocation pileups.

## 1. Introduction

Fatigue of materials is a subject of practical importance in engineering and has been widely studied (Bathias and Pineau, 2013; Broek, 1986; Schijve, 2009; Suresh, 1998). Fatigue refers to changes in material properties resulting from cyclic loading. Fatigue strength of crystalline materials is typically controlled by microcrack initiation and subsequent growth that leads to failure.

It is not surprising that fatigue appears to play an important role in sea ice mechanics. For example, the Arctic and Antarctic floating ice covers and ice shelves are subjected to cyclic loading from ocean swells that can penetrate deeply into an ice pack and potentially result in the breakup of the ice cover (Squire, 2007). Such events, where under the action of surface waves a floating ice cover exhibited sudden breakup into smaller pieces, have been repeatedly witnessed and described (Shackleton, 1982; Liu and others, 1988; Prinsenber and Peterson, 2011; Asplin and others, 2012; Collins and others, 2015; Kohout and others, 2016; Hwang and others, 2017). Ice cover breakup leads to a decline in albedo (Pistone and others, 2014; Zhang and others, 2019) and to the acceleration of melting. Also, smaller ice floes attenuate ocean waves less effectively than does the parent solid ice cover, thereby endangering coastal zones to erosion. Given the retreat of the sea ice cover and the attendant increase in oceanic fetch, larger waves are expected to develop; correspondingly, the remaining ice cover is expected to be subjected to episodes of greater cyclic loading. The potential for fatigue failure is thus increasing.

34  
35  
36  
37  
38  
39  
40  
41  
42  
43  
44  
45  
46  
47  
48  
49  
50  
51  
52  
53  
54  
55  
56  
57  
58  
59  
60  
61  
62  
63  
64  
65  
66  
67  
68  
69  
70

Cyclic loading may also play an important role in other scenarios. For instance, during ice-structure interactions (Jordaan, 2001; Hendrikse and Metrikine, 2016; O'Rourke and others, 2016; Jordaan and others, 2008) the structure itself, such as a light-house, may be weakened or damaged to a degree that depends on the strength of the ice. Other examples are runways and roads that are built by freezing water on cold oceans, rivers and lakes and subsequently subject to cyclic loading. Therefore, it is important to understand the behavior of ice under cyclic loading.

Currently, the effects of cyclic loading on the physical and mechanical properties of sea ice and on the susceptibility of the material to fatigue are poorly constrained. Tabata and Nohguchi (1980) conducted experiments on sea ice sampled from Lake Saroma, Hokkaido, Japan and from Barrow, Alaska. They loaded the ice cyclically under uniaxial compression between two specified stress levels under a variety of combinations of strain rate (from  $10^{-5} \text{ s}^{-1}$  to  $10^{-2} \text{ s}^{-1}$ ), temperature (from  $-2 \text{ }^{\circ}\text{C}$  to  $-24 \text{ }^{\circ}\text{C}$ ) and orientation (horizontal and vertical). They found that with a decrease of average stress and with a decrease of amplitude, the time to failure increases; and by lowering the temperature, the time to failure and the number of cycles also increases.

Other evidence of the weakening of sea ice under wave-driven in situ cyclic loading is discussed by Haskell and others (1996), Bond and Langhorne (1997), Langhorne and others (1998), (1999), (2001). In these works the authors obtained an S-N fatigue curve (S, upper peak stress of cycling; N, number of cycles imposed to failure), typical of curves obtained from engineering materials, i.e. for lower stress amplitude more cycles are needed for failure. The authors stated that the endurance limit, that is the stress amplitude below which the sea ice can withstand an unlimited number of cycles, is approximately one-half the failure stress of non-cycled ice.

The constitutive behavior of saline ice under cyclic loading was also investigated previously (Cole, 1995, 1998; Cole et al., 1998, 2002; Cole and Dempsey, 2004; Cole and Durell, 1995; Dempsey et al., 2003; Wei et al., 2020); specifically, inelastic deformation of sea ice was explored and interpreted in terms of a dislocation-based mechanism. In these works the authors investigated the effect of temperature (from  $-5$  to  $-50 \text{ }^{\circ}\text{C}$ ), microstructure (total porosity varied from 14 to 104 ppt), cyclic stress amplitude (from 0.04 to 0.8 MPa), loading frequency (from  $10^{-3}$  to 1 Hz), and dry isothermal vs floating specimens on the response of the ice. However, the strength of ice after it had been cycled was not measured.

Nothing more (to our knowledge) has been reported on the fatigue of sea ice. The topic is absent from a critical review by Squire (2007) and from two recent books on ice (Schulson and Duval, 2009; Weeks, 2010).

The behavior summarised above indicating the weakening of ice under cyclic loading, obtained from experiments conducted on saline and sea ice, might possibly account for the sudden breakup of natural ice covers. However, this behavior appears in conflict with the behavior of freshwater ice under cyclic loading (Cole, 1990;

71 Gupta et al., 1998; Iliescu et al., 2017; Iliescu and Schulson, 2002; Murdza et al., 2019, 2020b, 2020a). In those  
72 experiments, it was discovered that the ice flexural strength increases upon repetitive loading, followed by the  
73 recovery of the cyclic-induced increment in strength to the original non-cycled strength upon post-cycling annealing.  
74 This difference in the behavior of the two kinds of ice could perhaps be attributed to the presence of defects in  
75 sea/saline ice, such as brine pockets, brine channels and non-penetrating microcracks. Such defects serve as stress  
76 concentrators, thereby lessening the need to nucleate cracks to the degree that fatigue life may be governed primarily  
77 by crack propagation. The strengthening of ice is of more than scientific interest, reflected, perhaps in an interesting  
78 comment of an arctic engineer who reported that builders of ice roads never trust the ice until it had been “worked  
79 in” (Masterson, 2018).

80

81 Therefore, given that limited information about the behavior of sea/saline ice under cyclic loading and  
82 given the discrepancy in behavior of fresh and sea/saline ice, we conducted a study under controlled conditions in  
83 the laboratory on the flexural behavior of saline ice. In this paper, we describe the experiments in which beams of S2  
84 columnar-grained saline ice of two salinities ( $3.0 \pm 0.9$  and  $5.9 \pm 0.6$  ‰) were subjected at  $-10$  °C to four-point, reverse  
85 cycling at  $\sim 0.1$ - $0.6$  Hz and then, after several hundred or more cycles, were bent to failure, provided the beams did  
86 not break during cycling. We chose the rate of cycling to simulate the vibration frequency of a natural sea ice cover  
87 (Collins et al., 2015).

## 88 2. Experimental procedure

### 89 2.1 Ice growth and characterization

90 We studied saline ice of two melt-water salinities:  $3.0 \pm 0.9$  and  $5.9 \pm 0.6$  ppt, where  $\pm$  sign indicates standard  
91 deviation. We produced the ice in the laboratory in an 800 L circular polycarbonate tank in the manner described  
92 previously (Golding et al., 2014). Briefly, solutions containing  $17.5 \pm 0.2$  ppt and  $35 \pm 0.2$  ppt (parts per thousand,  
93 or ‰) of the commercial product “Instant Ocean” salt mixture were prepared and then frozen unidirectionally  
94 downward over a period of about 7 days by using a top-placed cold plate maintained at a temperature  $T = -$   
95  $20 \pm 0.1$  °C. Before bringing the cold plate into contact with the salt-water solution, the top surface of the solution  
96 was seeded with freshwater ice fragments of  $\sim 0.3$  - 1 mm in diameter. This procedure produced pucks  $\sim 1$  m in  
97 diameter and  $\sim 0.3$  m thick. For practical considerations, the bottom, skeletal layer of ice of about 7-10 cm was  
98 discarded as it was slushy and weak; we also believe that the skeletal layer does not play a significant role in  
99 supporting load. The top layer of ice of a few centimeters was also discarded because it was seeded and its grain size  
100 was considerably smaller and its microstructure thus different from the rest of the ice puck. Melt-water salinity was  
101 measured using a calibrated YSI Pro30 conductivity and salinity probe.

102

103 Figure 1 shows the microstructure of the ice. Table 1 lists its density and the average grain size of the test  
104 specimens described below. Figure 2 shows stereographic projections of the orientation of the crystallographic *c*-  
105 axes. The ice is characterized by columnar-shaped grains whose growth texture is marked by *c*-axes confined within

106 about 15° of the horizontal plane of the parent ice puck and randomly oriented within that plane. In other words, the  
107 ice is termed S2, after Michel and Ramseier (1971), and is similar to natural first-year sea ice (for comparison, see  
108 Figure 3.7 of Schulson and Duval (2009)). The grain size noted above is the average diameter of the columnar-shaped  
109 grains, ranging from about 2 to 7 mm in Figure 1.

## 110 **2.2. Growth features**

111 The ice contained both sub-mm sized brine pockets and supra-mm sized drainage channels, reminiscent of  
112 natural sea ice. Figures 3 and 4 show examples. The ice of lower salinity ( $3.0 \pm 0.9$  ppt) had fewer defects of both  
113 kinds. Some of the ice of higher salinity ( $5.9 \pm 0.6$  ppt) possessed channels whose size was almost as large as the  
114 grain diameter. The defects scattered light to the degree that in bulk form the ice had an overall opaque appearance.  
115 When observed in thin section ( $\sim 1$  mm) the ice exhibited to the naked eye distinct linear whitish features which we  
116 took to be sets of interconnected brine pockets that could possibly be filled with very fine-grained ice. The ice of  
117 higher salinity possessed more of these features, especially near the bottom of the parent puck (which was the last  
118 part to solidify). Our sense is that these features served as stress concentrators, particularly ones that traversed the  
119 width of the test specimen (described below), thereby weakening the ice. Indeed, as will become apparent, samples  
120 obtained from near the bottom of a puck of higher salinity ( $5.9 \pm 0.6$  ppt) had relatively low flexural strength.

121

122 Because the ice of both salinities exhibited a different appearance from the top and bottom of the parent  
123 puck, in preparing test specimens for flexing we distinguished them by their position (depth from top surface) within  
124 the ice puck from which they were prepared, Table 2.

## 125 **2.3. Sample preparation and test setup**

126 Once the ice had been grown, it was cut into blocks of dimensions  $\sim 10 \times 30 \times 20$  cm<sup>3</sup>, where the longest  
127 and the shortest dimensions are in the horizontal plane of the original ice puck, perpendicular to the direction of  
128 growth. The blocks were stored in a cooler (at  $-10 \pm 0.5$  °C) on their side (such that columnar-shaped grains were  
129 oriented horizontally) to reduce brine drainage for periods of time of about 1-10 weeks.

130

131 Specimens for flexing were manufactured from the ice blocks in the form of thin beams of dimensions  
132  $h \sim 16$  mm in thickness (parallel to the long axis of the grains),  $b \sim 85$  mm in width, and  $l \sim 300$  mm in length. The  
133 test specimens were allowed to equilibrate to the test temperature of  $-10 \pm 0.5$  °C for at least 24 hours before testing.

134

135 A detailed description of the specimens' preparation and loading can be found elsewhere (Iliescu et al.,  
136 2017; Murdza et al., 2018, 2019, 2020b). To summarize: The ice beams were flexed up and down under 4-point  
137 loading under constant displacement rate using a servo-hydraulic loading system (MTS model 810.14) to which we  
138 attached a custom-built 4-point loading frame, Figure 5. The hydraulic actuator was driven up and down under  
139 displacement control with the load limited in both directions. A load cell, calibrated for both tension and

140 compression, and a linear variable differential transformer (LVDT) gauge were used for measurements of load and  
141 displacement of the upper surface of the ice beam during cycling.

142

143 Acoustic emissions were recorded during cycling using a PCI-2 18-bit A/D system; its frequency response  
144 was 3 kHz–3 MHz and its minimum acoustic emission (AE) amplitude detection threshold was set to 45 dB. We  
145 used a micro 30STC sensor (9.5 mm diameter, 11 mm thickness) which was attached to the top surface of an ice  
146 beam with a rubber band. Vacuum grease was used as the coupling agent between the sensor and the ice surface.

147

148 The experiments were performed in a cold room at a temperature of -10°C and at an outer-fiber center-  
149 point displacement rate of 0.1 mm s<sup>-1</sup> (or outer-fiber strain rate of about 1.4 x 10<sup>-4</sup> s<sup>-1</sup>). This displacement rate  
150 resulted in an outer-fiber stress rate in the range from ~ 0.3 to 0.5 MPa s<sup>-1</sup>, outer-fiber stress amplitude in the range  
151 from 0.35 to 1.2 MPa, outer-fiber strain amplitude in the range from ~ 1 to 5 x 10<sup>-4</sup> and frequencies in the range  
152 from 0.1 to 0.6 Hz (i.e. periods from ~10 to 1.5 sec). The period, as already noted, is similar to the period of ocean  
153 swells (Collins et al., 2015). The major outer-fiber stress  $\sigma_f$  was calculated from the relationship (the loading span is  
154 ½ of the support span):

155

$$\sigma_f = \frac{3PL}{4bh^2} \quad (1)$$

156

157

158 where  $P$  is the applied load and  $L$  is the distance between the outer-pair of loading cylinders (shown in Figure 5b)  
159 and is set by the geometry of the apparatus to be  $L = 254$  mm.

160

161 We used two different loading procedures, as we did earlier in our study of S2 freshwater ice. Type I  
162 loading was a completely reversed stress cycle with constant stress amplitude and mean stress of zero. Type II was  
163 similar to Type I but incorporated an increasing multi-level (or step-level) stress amplitude. This second type of  
164 loading essentially consisted of several Type I steps of increasing stress amplitudes. In the present study for stress  
165 amplitudes below 0.7 MPa we used Type I loading. To cycle ice samples at stress amplitudes above 0.7 MPa, we  
166 first pre-conditioned specimens through step-loading Type II procedure at progressively higher stress amplitude  
167 levels, i.e. we cycled specimens for ~300 times at each of the following stress amplitudes: 0.7, 0.75, 0.8, 0.85 MPa  
168 and so on either until failure occurred or until a specific value of stress amplitude set by the operator (see Iliescu et  
169 al. (2017) and Murdza et al. (2018) for details). To change stress amplitude the loading was stopped for ~15 sec to  
170 change settings. After pre-conditioning, the specimens were cyclically loaded according Type I loading at least 300  
171 times and generally for ~2000 times, since no change in strength was observed beyond a few hundred cycles (see  
172 below).

173

174 Figure 6 shows measurements of load and of displacement versus time at the beginning and near the end of  
175 cycling before specimen failure of a lower-salinity specimen (3.0±0.9 ppt). The measurements detected no

176 softening. According to Bažant et al. (1984) softening is a decline of stress at increasing strain or, in our case, an  
177 increase of strain during cycling at constant stress amplitude during the tests). The absence of detectable softening  
178 during cycling of the saline ice is reminiscent of the absence of softening during the cycling of freshwater ice  
179 (Iliescu et al., 2017; Murdza et al., 2020b).

### 180 3. Results and Observations

#### 181 3.1. Flexural strength of non-cycled ice

182 The flexural strength of non-cycled saline ice of both salinities was measured at  $-10\text{ }^{\circ}\text{C}$  and at a nominal  
183 outer-fiber center-point displacement of  $0.1\text{ mm s}^{-1}$ . The results are listed in Table 2. Failure more often occurred at  
184 random locations between the two inner loading cylinders and less often either below or slightly outside the loading  
185 cylinders. The reason for the latter location was the presence prior to testing of a significant concentration of whitish  
186 features at loading cylinders which served as stress concentrators and along which the failure ultimately occurred  
187 (similar to Figure 4). The average and standard deviation of the measured flexural strength of saline ice of lower  
188 salinity ( $3.0\pm 0.9$  ppt) are  $0.96\pm 0.13$  MPa. The strength of the lower salinity ice did not correlate systematically with  
189 the depth of the parent puck from which ice beams were prepared. The measured strength compares favorably with  
190 the value of  $0.85\pm 0.20$  MPa reported by Timco and O'Brien (1994) for sea ice of similar salinity, as can be seen in  
191 Figure 7. Brine volume fraction  $v_b$  was calculated according to Frankenstein and Garner (1967):

192

$$v_b = 0.001 * S \left( \frac{49.185}{|T|} + 0.532 \right), \quad (2)$$

193

194 where  $T$  is temperature in degrees Celsius between  $-0.5\text{ }^{\circ}\text{C}$  and  $-22.9\text{ }^{\circ}\text{C}$  and  $S$  is melt-water salinity (in ppt) of the  
195 ice.

196

197 The average and standard deviation of the measured flexural strength of saline ice of higher salinity  
198 ( $5.9\pm 0.6$  ppt) are  $0.98\pm 0.36$  MPa. The measured values (Figure 7) deviate slightly towards higher values compared  
199 to the data of Timco and O'Brien (1994), although scatter is significantly greater than is the scatter in the strength of  
200 the ice of lower salinity ( $3.0\pm 0.9$  ppt). This may be explained by the greater degree of interconnectivity of brine  
201 pockets at the bottom of an ice puck (discussed above and shown in Figures 3 and 4). Indeed, the flexural strength of  
202 the higher-salinity specimens appears to depend on the depth of ice from which beams were prepared, Table 2. This  
203 result shows how much the strength of ice is sensitive to flaws and defects. Given that larger bodies usually contain  
204 larger defects, the flexural strength of sea ice on the medium and large scale, in the field (Karulina et al., 2019) for  
205 instance, is expected to be lower than on the smaller scale of the present experiments.

206

207 We also compare our measurements of flexural strength with the tensile strength of sea ice. For this  
208 purpose, and as we did in our previous work on freshwater ice (Iliescu et al., 2017; Murdza et al., 2020b), flexural

209 strength is divided by 1.7 (Ashby and Jones, 2012). This factor reflects the fact that the volume of the material  
 210 which is subjected to the highest stress in bending is smaller than in uniaxial tension; thus, the largest defect which  
 211 governs the failure may not be near the surface of a bent specimen. Upon dividing the flexural strength of the non-  
 212 cycled saline ice of lower salinity by 1.7, we found the average across-column tensile strength from our experiments  
 213 to be  $0.96 \pm 0.13 \text{ MPa} / 1.7 = 0.56 \pm 0.08 \text{ MPa}$ . This value compares favorably with the values  $0.56 \pm 0.06 \text{ MPa}$  and  
 214  $0.63 \pm 0.12 \text{ MPa}$  reported by Richter-Menge and Jones (1993) for the tensile strength of columnar-grained first-year  
 215 sea ice of  $4.1 \pm 0.3 \text{ ppt}$  salinity loaded uniaxially across the columns at a temperature of  $-10 \text{ }^\circ\text{C}$  and strain rates of  $10^{-5}$   
 216 and  $10^{-3} \text{ s}^{-1}$ . Recall that in the present experiments the outer-fiber strain rate was about  $1.4 \times 10^{-4} \text{ s}^{-1}$  which is within  
 217 the range reported by Richter-Menge and Jones (1993). This agreement between direct and indirect measurements of  
 218 tensile strength lends confidence that our lab-grown saline ice is a reasonably faithful analogue of natural sea ice.

### 219 3.2. Flexural strength versus number of reversed cycles under constant low stress amplitude

220 To determine whether there is a relationship between flexural strength and number of cycles imposed under  
 221 a constant low stress amplitude, we performed via Type-I loading a series of experiments on saline ice of lower  
 222 salinity ( $3.0 \pm 0.9 \text{ ppt}$ ) at  $-10 \text{ }^\circ\text{C}$  at an outer-fiber center-point displacement rate of  $0.1 \text{ mm s}^{-1}$  at a low stress  
 223 amplitude of  $0.35 \text{ MPa}$ ; i.e., at an amplitude less than one-half the flexural strength of non-cycled ice. Figure 8  
 224 shows the results. The number of cycles varied from about 100 to 14000. The average strength and standard  
 225 deviation of all data from Figure 8 are  $0.96 \pm 0.23 \text{ MPa}$ . As noted above the strength and standard deviation of non-  
 226 cycled ice are  $0.96 \pm 0.13 \text{ MPa}$ . In other words, no strengthening was detected upon cycling up to 14000 times at a  
 227 stress amplitude of  $0.35 \text{ MPa}$ . For freshwater ice (Murda et al., 2020b), we found that once the number of cycles at  
 228 a given low stress amplitude exceeded 300, the number of cycles had no significant effect on the flexural strength,  
 229 implying that a kind of saturation of strength developed. Given that result and the new results for saline ice, we  
 230 followed the practice in the present study of cycling more than 300 times, often as many as 2000 times, before  
 231 bending the ice to failure.

### 232 3.3. Flexural strength versus stress amplitude

233 The flexural strength increases with stress amplitude. Figure 9 shows measurements obtained from saline  
 234 ice of both salinities cycled at  $-10 \text{ }^\circ\text{C}$  at an outer-fiber displacement rate of  $0.1 \text{ mm s}^{-1}$ . For comparison, data from  
 235 laboratory grown freshwater ice (Murda et al., 2020b) of S2 character and from lake ice of the same character  
 236 (Murda et al., 2020a, 2021) are also shown. The relationship between the flexural strength,  $\sigma_{fc}$  and cycled stress  
 237 amplitude,  $\sigma_a$ , for saline ice appears to be a linear one and, within experimental scatter, to have essentially the same  
 238 sensitivity to stress amplitude as freshwater ice; namely:

$$239 \sigma_{fc} = \sigma_{f0} + k\sigma_a , \quad (3)$$

240

241 where  $k = 0.68$  is a constant. For freshwater ice the non-cycled flexural strength is  $\sigma_{f0} = 1.75$  MPa compared with  
242  $\sigma_{f0} = 0.96$  MPa for the saline ice. There is, perhaps, in Figure 9 a hint that for saline ice there is a threshold of  
243 about 0.4 MPa that must be exceeded to detect strengthening. Interestingly, this apparent threshold is similar in  
244 magnitude to the stress that marks the onset of significant AE activity under cyclic loading of sea ice cores (Cole  
245 and Dempsey, 2006). Although saline ice is weaker than freshwater ice, it appears that upon cycling its strength  
246 increases at the same rate as freshwater ice.

247  
248 Although the rate of strengthening with stress amplitude appears to be the same for saline ice and freshwater  
249 ice, the maximum increase in strength in the case of saline ice of lower salinity ( $3.0 \pm 0.9$  ppt) is significantly lower.  
250 We were able to strengthen saline ice by about 50% of the non-cycled strength compared with about 100% for  
251 freshwater ice (Murdza et al., 2020b). Another point is that we almost were not able to cycle specimens at stress  
252 amplitudes greater than the flexural strength of non-cycled material, whereas in the case of freshwater ice we were  
253 able to cycle at stress amplitudes significantly greater than flexural strength of non-cycled ice. Indeed, the maximum  
254 cycled stress amplitude we were able to reach in the case of saline ice of lower salinity ( $3.0 \pm 0.9$  ppt) during all tests  
255 was 1.1 MPa, which is not statistically different from the non-cycled flexural strength of  $0.96 \pm 0.13$  MPa.

256  
257 For saline ice of lower salinity ( $3.0 \pm 0.9$  ppt), there is no evidence that the flexural strength of both non-  
258 cycled and cycled ice is significantly affected by the depth of ice from which ice beams were harvested. For saline  
259 ice of higher salinity ( $5.9 \pm 0.6$  ppt), however, the flexural strength of both non-cycled and cycled ice appears to  
260 depend on the depth of ice from which beams were prepared, Figure 10. Indeed, the flexural strength of specimens  
261 from the bottom and from the top of an ice puck of higher salinity ( $5.9 \pm 0.6$  ppt) differs by  $\sim 3$  times ( $\sim 0.4$  MPa vs  
262  $\sim 1.4$  MPa).

### 263 3.4. Fatigue behavior

264 Although the specimens from which the data in Figure 9 were obtained did not fail during cycling, other  
265 specimens cycled under similar conditions did fail while being cycled. Results from such tests (on of saline ice of  
266 lower salinity ( $3.0 \pm 0.9$  ppt) at  $-10^\circ\text{C}$  and  $0.1 \text{ mm s}^{-1}$  outer-fiber displacement rate) allowed us to construct S-N  
267 fatigue curve, shown in Figure 11. The number of cycles here is the number of cycles to failure during cycling at  
268 the last stress amplitude level and not the total number of cycles. At most the S-N curve showd only a weak  
269 systematic dependence of the number of cycles to failure on stress amplitude. Indeed, for the same stress amplitude  
270 of  $\sim 0.9$  MPa, fatigue failure occurred after as few as  $<10$  cycles and after as many as a few thousand cycles.  
271 Statistical analyses to test the hypothesis that the slope in Figure 11 is zero resulted in a p-value equal  $\sim 0.06$ .  
272 Therefore, there is only a marginally significant effect of number of cycles on the stress at which failure occurred.  
273 We attribute this variability in fatigue life to the variability in microstructure from specimen to specimen.

274



275 That said, a note of caution is appropriate. The data in Figure 11 should not be viewed as fatigue data in the  
276 usual sense; i.e., in the way such data are viewed when obtained from other materials (e.g., metals and alloys) that  
277 exhibit classical fatigue behavior. In those cases, before cycling, all specimens are assumed to have the same  
278 thermal-mechanical history. That was not the case here for the saline ice, as most of the samples were pre-  
279 conditioned according to Type II procedure before they were cycled at the last stress level where they failed while  
280 cycling. In other words, in order to get fatigue failure, we were increasing stress amplitude by small increments of  
281 ~0.05 MPa and allowed a sufficient number of cycles at each stress level (~500-1000) before we reached a fatigue  
282 failure.

283  
284 The question to address here is why we did not obtain a classical S-N curve? We suggest that the classical  
285 mechanism of fatigue, i.e. accumulation of damage, is not in play in our tests and some other process is controlling  
286 fatigue life.

### 287 **3.5 Microstructural observations of samples after fatigue failure**

288 In an attempt to reveal deformation damage in the form of microcracks, we examined using thin-section  
289 optical microscopy (up to 50x magnification) the microstructure of specimens of the lower salinity ice ( $3.0\pm 0.9$  ppt)  
290 after they had failed during cycling; i.e., failed in fatigue. Three thin sections were prepared from four specimens in  
291 order to ensure a greater probability of observing microcracks growing from brine pockets or brine channels, should  
292 they be present. The plane of the thin section was parallel to the long axis of the columnar grains and parallel to the  
293 direction of the greater normal stress. This plane was taken as the best plane to observe possible cracks. Thin  
294 sections were observed using non-polarized light. We found no evidence of microcracks starting from brine pockets  
295 or from other defects. In fact, we found no microcracks at all. It appears, therefore, that slow crack growth is not a  
296 significant contribution to the fatigue life of the beams of the laboratory-grown saline ice that we studied.

### 297 **3.6. Acoustic emissions**

298 Acoustic emissions (AE) during repetitive loading of ice have been previously recorded and analyzed in  
299 laboratory and in situ (Langhorne and Haskell, 1996), (Cole and Dempsey, 2006, 2004; Lishman et al., 2020;  
300 Murdza et al., 2020b). Langhorne and Haskell (1996) suggested that the emissions originate either from dislocation  
301 breakaway or from microcracking associated with dislocation motion.

302  
303 In contrast to freshwater ice, where no sound was detected until failure (Murdza et al., 2020b), continuous  
304 emission was detected while cycling at constant stress amplitude. Figure 12 shows the cumulative acoustic  
305 emissions, or “hits”, as a function of time for ice that was cycled reversely at a constant stress amplitude of 0.5 MPa.  
306 As can be seen, the hit rate (or hits per unit time), which is the slope of the curve in Figure 12, is about the same for  
307 the duration of the experiment.

308

309 Interestingly, the hit rate depends on stress amplitude during cycling. Figure 13 shows this behavior . The  
310 greater is the stress amplitude, the greater is the hit rate. However, during cycling below about 0.2 MPa no hits were  
311 detected.

312

313 Figure 13 also indicates that the hit rate is independent of the sequence of different stress amplitudes. The  
314 numbers in Figure 13 show the order of cycling at different stress amplitudes; i.e., firstly we cycled ice at higher  
315 stress amplitudes (0.5-0.8 MPa), then at lower stress amplitudes (0.2-0.4 MPa). The results showed an increase in  
316 the hit rate as stress amplitude increases, regardless of the sequence of cycling.

#### 317 **4. Discussion**

318 The results obtained from the experiments described in this paper show that the flexural strength of saline  
319 ice can be increased upon reversed cyclic loading. Therefore, the same set of questions as for the freshwater ice  
320 should be addressed here, i.e.: What governs the flexural strength of saline ice? Does crack propagation or crack  
321 nucleation control the tensile strength? First of all, to understand the behavior of saline ice, it is important to  
322 recognize that flexural strength in the present experiments is governed by the tensile strength, although greater by a  
323 factor of about 1.7 (Ashby and Jones, 2012). Secondly, the apparent absence of remnant microcracks within the two  
324 parts of broken samples (Section 3.5) indicates that crack nucleation controls the flexural strength, just as it appears  
325 to do for freshwater ice. Indeed, this seems reasonable given the fact that freshwater ice comprises of ~95% by  
326 volume of the saline ice we studied. Within the freshwater component, there is almost no solubility of salts (Weeks  
327 and Ackley, 1986). The remainder of the saline ice is a mixture of air and brine. As was shown earlier, the  
328 microstructure of saline ice that we grew is closely similar to the microstructure of sea ice. Pores lower the saline ice  
329 strength (Sammis and Ashby, 1986). However, the behavior of S2 saline ice under cyclic loading is essentially the  
330 same as the behavior of S2 freshwater ice (Murda et al., 2020b), i.e. its strength increases at the same rate as  
331 freshwater ice upon cycling under a given amplitude of the outer fiber stress. Hence, it is reasonable to assume that  
332 the strengthening mechanism for the saline ice is similar to that for the freshwater ice. In our earlier work (Murda  
333 et al., 2020b) we proposed that strengthening might be due to the development of an internal back stress that  
334 originates from either dislocation pileups or grain boundary sliding. However, one reviewer suggested the  
335 possibility of a different strengthening mechanism. Due to the inherent weakness of the saline ice microstructure, the  
336 microstructural stress relief may occur through localized damage via microcracking mentioned above. More  
337 research, however, is needed to examine this hypothesis.

338

339 The maximum degree of strengthening in the case of saline ice is significantly lower than that for the  
340 freshwater ice, although the slopes of the two data sets (rate of strength increase with increasing cyclic amplitude) in  
341 Figure 9 are nearly equivalent. That difference may be explained by the structure of saline ice which limits  
342 maximum possible strengthening. Given the significantly greater number of stress concentrators in saline ice, such  
343 as brine pockets and channels, the propensity for failure during cycling is greater in saline ice (Sammis and Ashby,

344 1986), thereby limiting the development of the back stress. Indeed, in the present study failure of specimens during  
345 cycling occurred more frequently than in the study on freshwater ice (Murdza et al., 2020b).

346  
347 Flexural experiments conducted on saline ice of higher salinity ( $5.9\pm 0.6$  ppt) showed the importance of  
348 brine features. Samples that were manufactured from the bottom of the ice puck were characterized by more  
349 frequent whitish interconnected features (taken to be interconnected brine pockets) that often were the path for easy  
350 crack propagation. Often samples were so weak that they failed before testing simply by handling. Interestingly,  
351 there were no interconnected features in samples prepared from the top of an ice puck, which resulted in a difference  
352 of more than a factor of three in strength between samples from top and bottom. Samples produced from saline ice  
353 of lower salinity ( $3.0\pm 0.9$  ppt) also had whitish features; however, these features were spread more uniformly (on a  
354 macroscopic scale) across the sample, resulting in little difference in strength between the bottom and top samples.

355  
356 It is worth noting again that a significantly greater fraction of saline ice samples failed in fatigue while pre-  
357 conditioning compared with freshwater ice. This may be explained by the fact that freshwater ice was essentially  
358 free from pores, brine pockets and other defects. Based on this observation, it appears that crack growth is not a  
359 significant contribution to the fatigue life of saline ice under the conditions of our experiments.

360  
361 On the origin of the acoustic emissions, there are at least four possible sources of the noise detected. One is  
362 from microcracking. We imagine that microcracks form in regions of mechanical weakness which results in  
363 accumulation of damage that we detected via the AE method. Specifically, the brine drainage whitish features  
364 discussed above in the test specimens constitute regions of high porosity and thus provide favorable sites for the  
365 concentration of such damage. Failure may occur when one of these sites can no longer support the applied stress  
366 and a microcrack emerges from the damage zone and propagates. It is possible that newly formed microcracks are  
367 stable until a critical length is reached (Cannon et al., 1990; Schulson et al., 1991), at which point the crack growth  
368 ensues. The reason that microcracks were not observed under the optical microscope may be because they filled up  
369 with liquid brine upon formation which results in a loss of contrast. A second possible explanation for the acoustic  
370 emissions is the motion and friction of very fine particles of ice which may have been entrapped inside brine  
371 drainage features, as mentioned above. A third possibility is microcracking along grain boundaries due to grain  
372 boundary sliding (Elvin and Shyam Sunder, 1996; Goldsby and Kohlstedt, 1997; Mulmule and Dempsey, 1997;  
373 Schulson et al., 1997; Weiss and Schulson, 2000). A fourth possible explanation consistent with the non-history  
374 dependence of the hit rate (Figure 13) is a kind of water-hammer effect in which brine entrapped within pockets  
375 impacts the wall, first in one direction and then another. None of these possibilities can be evaluated based upon the  
376 limits of the present observations. We refrain, therefore, from further speculation on this point.

377  
378 Returning to the observations noted in the Introduction, and to the results obtained from imposed, in situ  
379 cyclic loading experiments on sea ice beams by (Bond and Langhorne, 1997; Haskell et al., 1996; Langhorne et al.,  
380 1998, 1999), the question is: Why does ice fail in the field under wave action and under imposed cyclic loading, but

381 strengthen upon cycling in our experiments in the laboratory? Although we do not know the process through which  
382 the ice sheet failed in the field, we expect that there are many micro and macro cracks in natural sea ice. Indeed,  
383 thermally-induced tensile stresses can induce thermal cracking in floating ice sheets (Evans and Untersteiner, 1971).  
384 Therefore, our sense is that the difference in ice behavior under cyclic loading in situ in the field (Bond and  
385 Langhorne, 1997; Langhorne et al., 1998) and in the laboratory in the present study is due to other types of defects  
386 other than brine channels and pockets that are generated in the field as a result of thermo-mechanical history of ice.

## 387 **5. Conclusions**

388 From new, systematic experiments on the flexural strength of sub-meter sized beams of S2 columnar-  
389 grained saline ice stressed principally across the columns through reversed cyclic loading at a temperature of -10 °C  
390 and frequencies in the range from 0.1 to 0.6 Hz, it is concluded that:

- 391 (i) The flexural strength of saline ice can be increased upon reversed cyclic loading by as much as 1.5 times.
- 392 (ii) The flexural strength of ice subsequent to cycling scales linearly with the amplitude of the outer-fiber  
393 stress.
- 394 (iii) The fatigue life of saline ice is erratic and does not obey classical S-N behavior.
- 395 (iv) Crack growth is not a significant contribution to the fatigue life of saline ice.
- 396 (v) There is high variability in structure and strength through the thickness of a saline ice puck of higher  
397 salinity ( $5.9 \pm 0.6$  ppt).
- 398 (vi) Given the lack of definitive proof of the underlying failure mechanism in saline ice, the increase in flexural  
399 strength of freshwater ice and saline ice attributable to pre-failure load cycling is roughly equivalent.
- 400 (vii) Acoustic emission hit rate during cycling at a constant stress amplitude is about constant.
- 401 (viii) Acoustic emission hit rate during cycling increases with an increase of stress amplitude of cycling.

## 402 **Acknowledgements**

403 We acknowledge helpful discussions/communications with Prof. Harold Frost, Dr. Robert Gagnon, and  
404 Dr. Daniel Iliescu. We acknowledge thoughtful and helpful critical comments from two anonymous reviewers. This  
405 work was supported by the US Department of the Interior-Bureau of Safety and Environmental Enforcement  
406 (BSEE), contract no. E16PC00005 and by National Science Foundation (FAIN 1947-107).

407

408 **Author contributions:** AM, ES and CR designed the experiments and AM carried them out. AM prepared the  
409 manuscript with contributions from all co-authors.

410

411 **Competing interests:** The authors declare that they have no conflict of interest.

412 **References**

- 413 Ashby, M. M. and Jones, D. R. H.: Engineering Materials 1: An Introduction to Properties, Applications and  
414 Design., 2012.
- 415 Asplin, M. G., Galley, R., Barber, D. G. and Prinsenberg, S.: Fracture of summer perennial sea ice by ocean swell as  
416 a result of Arctic storms, *J. Geophys. Res. Ocean.*, 117(6), 1–12, doi:10.1029/2011JC007221, 2012.
- 417 Bathias, C. and Pineau, A.: *Fatigue of Materials and Structures*, edited by C. Bathias and A. Pineau, John Wiley &  
418 Sons, Inc., Hoboken, NJ, USA., 2013.
- 419 Bažant, Z. P., Belytschko, T. B. and Chang, T.: Continuum Theory for Strain-Softening, *J. Eng. Mech.*, 110(12),  
420 1666–1692, doi:10.1061/(asce)0733-9399(1984)110:12(1666), 1984.
- 421 Bond, P. E. and Langhorne, P. J.: Fatigue behavior of cantilever beams of saline ice, *J. Cold Reg. Eng.*, 11(2), 99–  
422 112, doi:10.1061/(ASCE)0887-381X(1997)11:2(99), 1997.
- 423 Broek, D.: *Elementary engineering fracture mechanics*, 1st ed., Springer, Dordrecht., 1986.
- 424 Cannon, N. P., Schulson, E. M., Smith, T. R. and Frost, H. J.: Wing cracks and brittle compressive fracture, *Acta*  
425 *Metall. Mater.*, 38(10), 1955–1962, doi:10.1016/0956-7151(90)90307-3, 1990.
- 426 Cole, D. and Dempsey, J.: Laboratory observations of acoustic emissions from antarctic first-year sea ice cores  
427 under cyclic loading, in 18th International POAC Conference, p. Vol 3, 1083-1092., 2006.
- 428 Cole, D. M.: Reversed direct-stress testing of ice: Initial experimental results and analysis, *Cold Reg. Sci. Technol.*,  
429 18(3), 303–321, doi:10.1016/0165-232X(90)90027-T, 1990.
- 430 Cole, D. M.: A model for the anelastic straining of saline ice subjected to cyclic loading, *Philos. Mag. A*, 72(1),  
431 231–248, doi:10.1080/01418619508239592, 1995.
- 432 Cole, D. M.: Modeling the cyclic loading response of sea ice, *Int. J. Solids Struct.*, 35(31–32), 4067–4075,  
433 doi:10.1016/S0020-7683(97)00301-6, 1998.
- 434 Cole, D. M. and Dempsey, J. P.: In situ Sea Ice Experiments in McMurdo Sound: Cyclic Loading, Fracture, and  
435 Acoustic Emissions, *J. Cold Reg. Eng.*, 18(4), 155–174, doi:10.1061/(ASCE)0887-381X(2004)18:4(155), 2004.
- 436 Cole, D. M. and Durell, G. D.: The cyclic loading of saline ice, *Philos. Mag. A Phys. Condens. Matter, Struct.*  
437 *Defects Mech. Prop.*, 72(1), 209–229, doi:10.1080/01418619508239591, 1995.
- 438 Cole, D. M., Johnson, R. A. and Durell, G. D.: Cyclic loading and creep response of aligned first-year sea ice, *J.*  
439 *Geophys. Res. Ocean.*, 103(C10), 21751–21758, doi:10.1029/98JC01265, 1998.
- 440 Cole, D. M., Dempsey, J., Kjestveit, G., Shapiro, S., Shapiro, L. and Morley, G.: The cyclic and fracture response of  
441 sea ice in McMurdo Sound. Part I, in *Proceedings of the 16th IAHR International Symposium on Ice*, Dunedin, New  
442 Zealand., 2002.
- 443 Collins, C. O., Rogers, W. E., Marchenko, A. and Babanin, A. V.: In situ measurements of an energetic wave event  
444 in the Arctic marginal ice zone, *Geophys. Res. Lett.*, 42(6), 1863–1870, doi:10.1002/2015GL063063, 2015.
- 445 Dempsey, J., Cole, D. M., Shapiro, S., Kjestveit, G., Shapiro, L. and Morley, G.: The cyclic and fracture response of  
446 sea ice in McMurdo Sound. Part II, in *Proceedings of the 17th International Conference on Port and Ocean*  
447 *Engineering under Arctic Conditions*, Trondheim, Norway. [online] Available from:  
448 [https://www.researchgate.net/publication/303460064\\_The\\_cyclic\\_and\\_fracture\\_response\\_of\\_sea\\_ice\\_in\\_McMurdo](https://www.researchgate.net/publication/303460064_The_cyclic_and_fracture_response_of_sea_ice_in_McMurdo)

449 \_Sound\_Part\_II (Accessed 14 January 2020), 2003.

450 Elvin, A. A. and Shyam Sunder, S.: Microcracking due to grain boundary sliding in polycrystalline ice under  
451 uniaxial compression, *Acta Mater.*, 44(1), 43–56, doi:10.1016/1359-6454(95)00157-1, 1996.

452 Evans, R. J. and Untersteiner, N.: Thermal cracks in floating ice sheets, *J. Geophys. Res.*, 76(3), 694–703,  
453 doi:10.1029/JC076i003p00694, 1971.

454 Frankenstein, G. and Garner, R.: Equations for Determining the Brine Volume of Sea Ice from  $-0.5^{\circ}$  to  $-22.9^{\circ}\text{C}$ ., *J.*  
455 *Glaciol.*, 6(48), 943–944, doi:10.3189/S0022143000020244, 1967.

456 Golding, N., Snyder, S. A., Schulson, E. M. and Renshaw, C. E.: Plastic faulting in saltwater ice, *J. Glaciol.*,  
457 60(221), 447–452, doi:10.3189/2014JoG13J178, 2014.

458 Goldsby, D. L. and Kohlstedt, D. L.: Grain boundary sliding in fine-grained ice I, *Scr. Mater.*, 37(9), 1399–1406,  
459 doi:10.1016/S1359-6462(97)00246-7, 1997.

460 Gupta, V., Bergström, J. and Picu, C. R.: Effect of step-loading history and related grain-boundary fatigue in  
461 freshwater columnar ice in the brittle deformation regime, *Philos. Mag. Lett.*, 77(5), 241–247,  
462 doi:10.1080/095008398178372, 1998.

463 Haskell, T. G., Robinson, W. H. and Langhorne, P. J.: Preliminary results from fatigue tests on in situ sea ice beams,  
464 *Cold Reg. Sci. Technol.*, 24(2), 167–176, doi:10.1016/0165-232X(95)00015-4, 1996.

465 Hendrikse, H. and Metrikine, A.: Edge indentation of ice with a displacement-controlled oscillating cylindrical  
466 structure, *Cold Reg. Sci. Technol.*, 121, 100–107, doi:10.1016/j.coldregions.2015.10.013, 2016.

467 Hwang, B., Wilkinson, J., Maksym, E., Graber, H. C., Schweiger, A., Horvat, C., Perovich, D. K., Arntsen, A. E.,  
468 Stanton, T. P., Ren, J. and Wadhams, P.: Winter-to-summer transition of Arctic sea ice breakup and floe size  
469 distribution in the Beaufort Sea, *Elem Sci Anth*, 5, 40, doi:10.1525/elementa.232, 2017.

470 Iliescu, D. and Schulson, E. M.: Brittle compressive failure of ice: Monotonic versus cyclic loading, *Acta Mater.*,  
471 50(8), 2163–2172, doi:10.1016/S1359-6454(02)00060-5, 2002.

472 Iliescu, D., Murdza, A., Schulson, E. M. and Renshaw, C. E.: Strengthening ice through cyclic loading, *J. Glaciol.*,  
473 63(240), 663–669, doi:10.1017/jog.2017.32, 2017.

474 Jordaan, I. J.: Mechanics of ice–structure interaction, *Eng. Fract. Mech.*, 68(17–18), 1923–1960, doi:10.1016/S0013-  
475 7944(01)00032-7, 2001.

476 Jordaan, I. J., Xiao, J., Wells, J. and Derradji-Aouat, A.: Ice crushing and cyclic loading in compression, in 19th  
477 IAHR International Symposium on Ice, pp. 1097–1106., 2008.

478 Karulina, M., Marchenko, A., Karulin, E., Sodhi, D., Sakharov, A. and Chistyakov, P.: Full-scale flexural strength  
479 of sea ice and freshwater ice in Spitsbergen Fjords and North-West Barents Sea, *Appl. Ocean Res.*, 90,  
480 doi:10.1016/j.apor.2019.101853, 2019.

481 Kohout, A. L., Williams, M. J. M., Toyota, T., Lieser, J. and Hutchings, J.: In situ observations of wave-induced sea  
482 ice breakup, *Deep. Res. Part II Top. Stud. Oceanogr.*, 131, 22–27, doi:10.1016/j.dsr2.2015.06.010, 2016.

483 Langhorne, P. J. and Haskell, T. G.: Acoustic emission during fatigue experiments on first year sea ice, *Cold Reg.*  
484 *Sci. Technol.*, 24(3), 237–250, doi:10.1016/0165-232X(95)00021-3, 1996.

485 Langhorne, P. J., Squire, V. A., Fox, C. and Haskell, T. G.: Break-up of sea ice by ocean waves, *Ann. Glaciol.*, 27,

486 438–442, doi:10.3189/S0260305500017869, 1998.

487 Langhorne, P. J., Squire, V. A. and Haskell, T. G.: Role of fatigue in wave-induced break-up of sea ice- a review, in

488 Ice in Surface Waters: Proceedings of the 14th International Symposium on Ice, pp. 1019–1023, Rotterdam, The

489 Netherlands., 1999.

490 Langhorne, P. J., Squire, V. A., Fox, C. and Haskell, T. G.: Lifetime estimation for a land-fast ice sheet subjected to

491 ocean swell, *Ann. Glaciol.*, 33, 333–338, doi:10.3189/172756401781818419, 2001.

492 Lishman, B., Marchenko, A., Sammonds, P. and Murdza, A.: Acoustic emissions from in situ compression and

493 indentation experiments on sea ice, *Cold Reg. Sci. Technol.*, 172, 102987, doi:10.1016/j.coldregions.2019.102987,

494 2020.

495 Liu, A. K., Mollo-Christensen, E., Liu, A. K. and Mollo-Christensen, E.: Wave Propagation in a Solid Ice Pack, *J.*

496 *Phys. Oceanogr.*, 18, 1702–1712, doi:10.1175/1520-0485(1988)018<1702:WPIASI>2.0.CO;2, 1988.

497 Masterson, D.: *The Story of Offshore Arctic Engineering - Dan Masterson* - Google Books, Cambridge Scholars

498 Publishing. [online] Available from:

499 [https://books.google.com/books/about/The\\_Story\\_of\\_Offshore\\_Arctic\\_Engineering.html?id=y9N1DwAAQBAJ](https://books.google.com/books/about/The_Story_of_Offshore_Arctic_Engineering.html?id=y9N1DwAAQBAJ)

500 (Accessed 4 March 2021), 2018.

501 Michel, B. and Ramseier, R. O.: Classification of river and lake ice, *Can. Geotech. J.*, 8(1), 36–45, doi:10.1139/t71-

502 004, 1971.

503 Mulmule, S. V. and Dempsey, J. P.: Stress-Separation Curves for Saline Ice Using Fictitious Crack Model, *J. Eng.*

504 *Mech.*, 123(8), 870–877, doi:10.1061/(asce)0733-9399(1997)123:8(870), 1997.

505 Murdza, A., Schulson, E. M. and Renshaw, C. E.: Hysteretic behavior of freshwater ice under cyclic loading :

506 preliminary results, in 24th IAHR International Symposium on Ice, pp. 185–192, Vladivostok., 2018.

507 Murdza, A., Schulson, E. M. and Renshaw, C. E.: The effect of cyclic loading on the flexural strength of columnar

508 freshwater ice, in Proceedings of the International Conference on Port and Ocean Engineering under Arctic

509 Conditions, POAC, vol. 2019-June., 2019.

510 Murdza, A., Marchenko, A., Schulson, E., Renshaw, C., Sakharov, A., Karulin, E. and Chistyakov, P.: Results of

511 preliminary cyclic loading experiments on natural lake ice and sea ice, in 25th IAHR International Symposium on

512 Ice, pp. 1–10, Trondheim, Norway., 2020a.

513 Murdza, A., Schulson, E. M. and Renshaw, C. E.: Strengthening of columnar-grained freshwater ice through cyclic

514 flexural loading, *J. Glaciol.*, 66(258), 556–566, doi:10.1017/jog.2020.31, 2020b.

515 Murdza, A., Marchenko, A., Schulson, E. M. and Renshaw, C. E.: Cyclic strengthening of lake ice, *J. Glaciol.*,

516 67(261), 182–185, doi:10.1017/jog.2020.86, 2021.

517 O’Rourke, B. J., Jordaan, I. J., Taylor, R. S. and Gürtner, A.: Experimental investigation of oscillation of loads in ice

518 high-pressure zones, part 1: Single indenter system, *Cold Reg. Sci. Technol.*, 124, 25–39,

519 doi:10.1016/J.COLDREGIONS.2015.12.005, 2016.

520 Pistone, K., Eisenman, I. and Ramanathan, V.: Observational determination of albedo decrease caused by vanishing

521 Arctic sea ice, *Proc. Natl. Acad. Sci. U. S. A.*, 111(9), 3322–3326, doi:10.1073/pnas.1318201111, 2014.

522 Prinsenbergh, S. J. and Peterson, I. K.: Observing regional-scale pack-ice decay processes with helicopter-borne

523 sensors and moored upward-looking sonars, *Ann. Glaciol.*, 52(57), 35–42, doi:10.3189/172756411795931688,  
524 2011.

525 Richter-Menge, J. A. and Jones, K. F.: The tensile strength of first-year sea ice, *J. Glaciol.*, 39(133), 609–618,  
526 doi:10.3189/S0022143000016506, 1993.

527 Sammis, C. G. and Ashby, M. F.: The failure of brittle porous solids under compressive stress states, *Acta Metall.*,  
528 34(3), 511–526, doi:10.1016/0001-6160(86)90087-8, 1986.

529 Schijve, J.: *Fatigue of Structures and Materials*, 2nd ed., Springer Netherlands., 2009.

530 Schulson, E. M. and Duval, P.: *Creep and Fracture of Ice*, Cambridge University Press, Cambridge., 2009.

531 Schulson, E. M., Kuehn, G. A., Jones, D. A. and Fifolt, D. A.: The growth of wing cracks and the brittle  
532 compressive failure of ice, *Acta Metall. Mater.*, 39(11), 2651–2655, doi:10.1016/0956-7151(91)90081-B, 1991.

533 Schulson, E. M., Qi, S., Melton, J. S. and Gratz, E. T.: Across-column cracks and axial splits in S2 saline ice under  
534 compression, *J. Glaciol.*, 43(145), 411–414, doi:10.3189/s0022143000034997, 1997.

535 Shackleton, E. H.: *South: The Story of Shackleton’s Last Expedition, 1914–17*, Macmillian, USA., 1982.

536 Squire, V. A.: Of ocean waves and sea-ice revisited, *Cold Reg. Sci. Technol.*, 49(2), 110–133,  
537 doi:10.1016/j.coldregions.2007.04.007, 2007.

538 Suresh, S.: *Fatigue of Materials*, Cambridge University Press., 1998.

539 Tabata, T. and Nohguchi, Y.: Failure of Sea Ice by Repeated Compression, in *Physics and Mechanics of Ice*, pp.  
540 351–362, Springer Berlin Heidelberg, Berlin, Heidelberg., 1980.

541 Timco, G. W. and O’Brien, S.: Flexural strength equation for sea ice, *Cold Reg. Sci. Technol.*, 22(3), 285–298,  
542 doi:10.1016/0165-232X(94)90006-X, 1994.

543 Weeks, W. F.: *On Sea Ice*, University of Alaska Press., 2010.

544 Weeks, W. F. and Ackley, S. F.: The Growth, Structure, and Properties of Sea Ice, in *The Geophysics of Sea Ice*, pp.  
545 9–164, Springer US, Boston, MA., 1986.

546 Wei, M., Polojärvi, A., Cole, D. M. and Prasanna, M.: Strain response and energy dissipation of floating saline ice  
547 under cyclic compressive stress, *Cryosph.*, 14(9), 2849–2867, doi:10.5194/tc-14-2849-2020, 2020.

548 Weiss, J. and Schulson, E. M.: Grain-boundary sliding and crack nucleation in ice, *Philos. Mag. A*, 80(2), 279–300,  
549 doi:10.1080/01418610008212053, 2000.

550 Zhang, R., Wang, H., Fu, Q., Rasch, P. J. and Wang, X.: Unraveling driving forces explaining significant reduction  
551 in satellite-inferred Arctic surface albedo since the 1980s, *Proc. Natl. Acad. Sci. U. S. A.*, 116(48), 23947–23953,  
552 doi:10.1073/pnas.1915258116, 2019.

553

554

555

556

557

558

559



560  
 561  
 562  
 563  
 564  
 565  
 566

**Table 1. Physical properties of as-grown saline ice.**

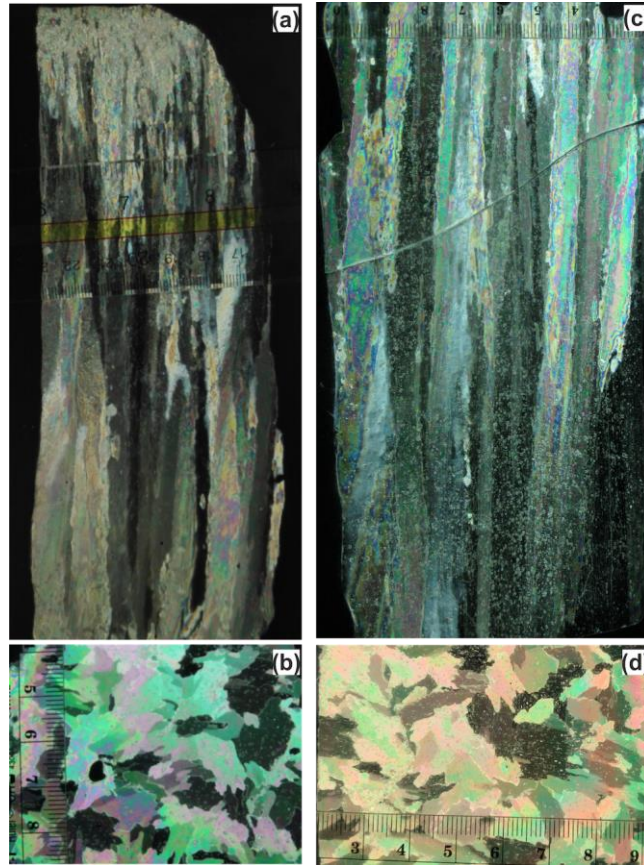
Material	Density [kg m <sup>-3</sup> ]	Average salinity [ppt]	Grain size [mm]
Saline ice (lower salinity)	878±11	3.0±0.9	3.8±0.9
Saline ice (higher salinity)	897±10	5.9±0.6	3.6±1.1

567  
 568  
 569  
 570

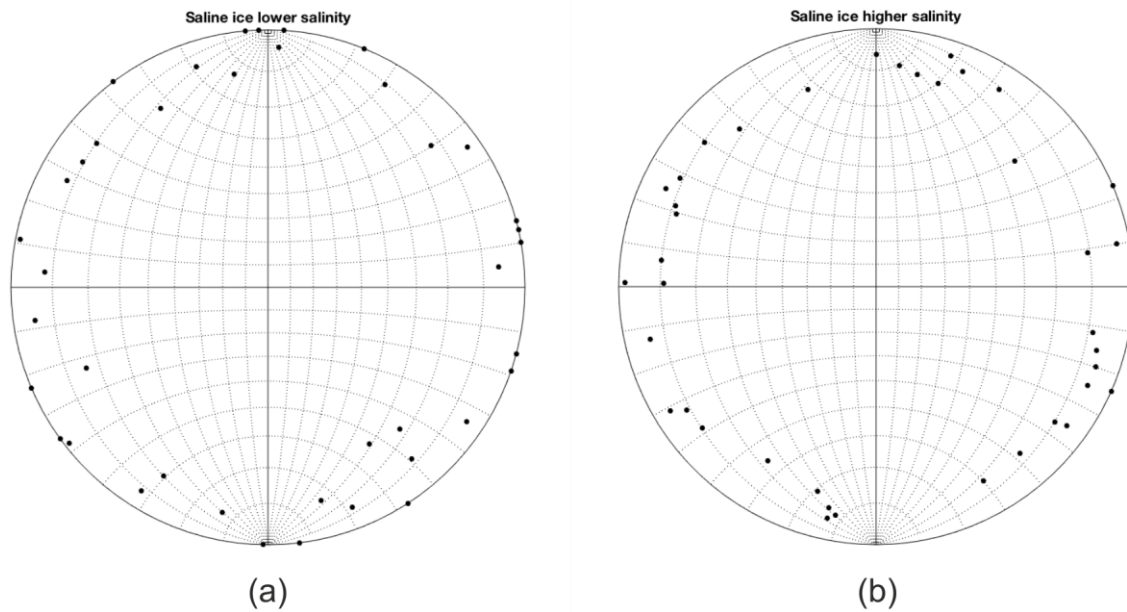
571 **Table 2. Flexural strength of non-cycled saline ice at -10°C and a displacement rate of 0.1 mm/s.**

Flex strength of ice of lower salinity (3.0±0.9 ppt) [MPa]	Depth [cm]	Flex strength of ice of higher salinity (5.9±0.6 ppt) [MPa]	Depth [cm]
1.08	—	0.45	20 – 22.5
0.86	—	0.53	17.5 – 20
1.06	—	0.62	12.5 – 15
0.96	—	0.98	7.5 – 10
0.83	17 – 21	1.17	5 – 7.5
0.75	13.5 – 17	1.26	5 – 7.5
1.08	10 – 13.5	1.26	2.5 – 5
0.97	6.5 – 10	1.44	1 – 2.5
1.09	3 – 6.5	1.17	—
Average		Average	
0.96±0.13		0.98±0.36	

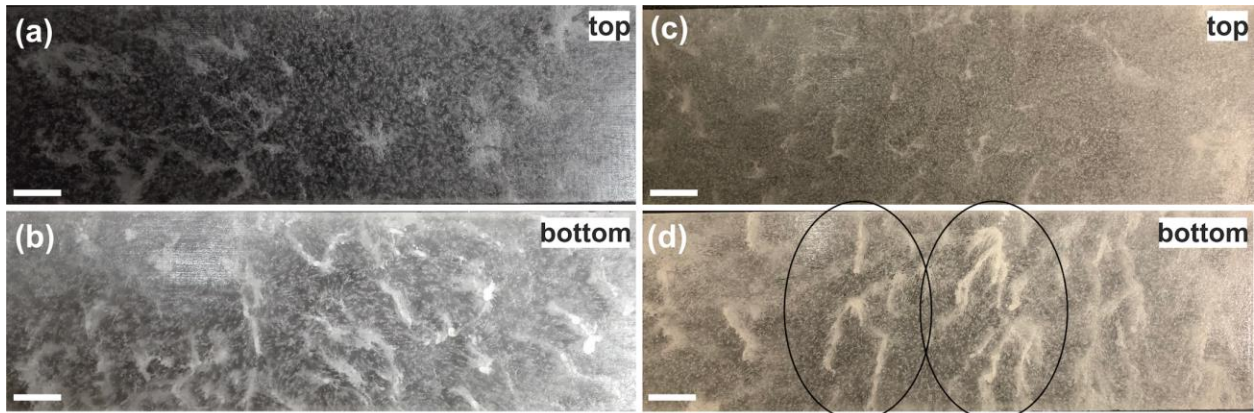
572  
 573



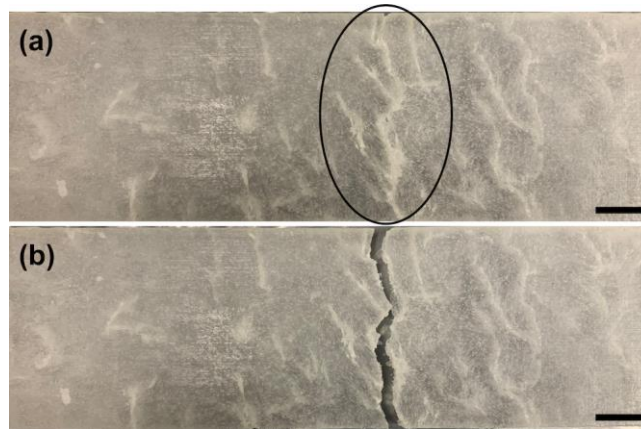
574  
 575 **Figure 1.** Photographs of a vertically-oriented (a) and a horizontally-oriented (b) thin-sections (~1mm) of columnar-  
 576 grained, saline ice of lower salinity ( $3.0 \pm 0.9$  ppt) as viewed between crossed-polarized filters; photographs of a vertically-  
 577 oriented (c) and a horizontally-oriented (d) thin-sections of saline ice of higher salinity ( $5.9 \pm 0.6$  ppt).



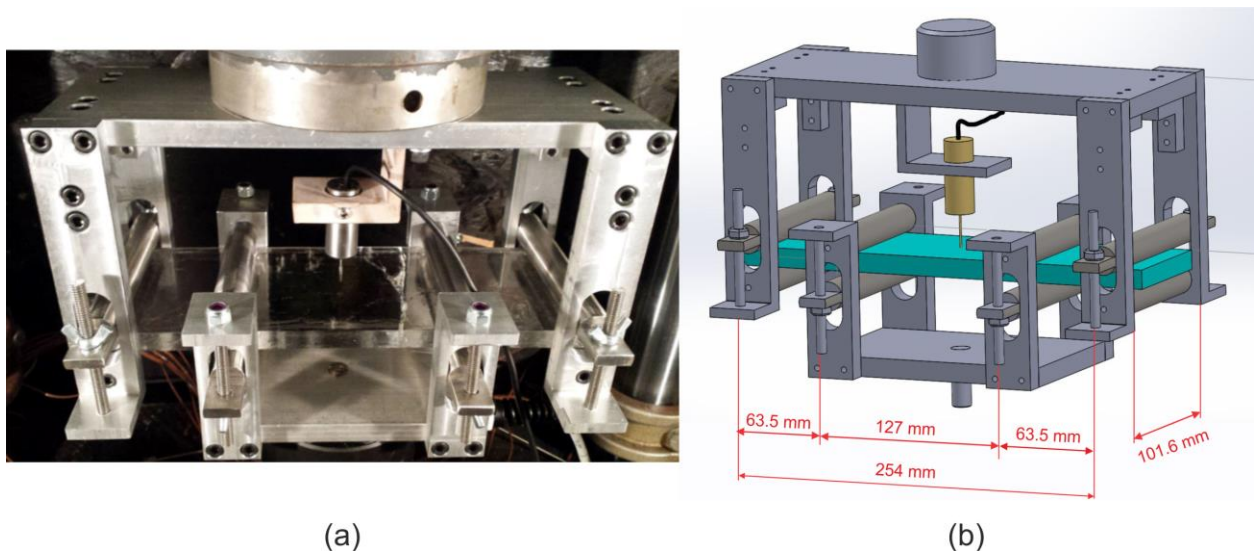
578  
 579 **Figure 2.** Stereographic projection plots of crystal c-axis {0001} orientations in saline ice of lower ( $3.0 \pm 0.9$  ppt) salinity (a)  
 580 and saline ice of higher ( $5.9 \pm 0.6$  ppt) salinity (b).



581  
582 **Figure 3.** Photographs of saline ice samples of lower salinity ( $3.0\pm 0.9$  ppt) from the top (a) and bottom (b) of an ice block  
583 and saline ice samples of higher salinity ( $5.9\pm 0.6$  ppt) from the top (c) and bottom (d) of an ice block. The concentration of  
584 whitish features along the width of a sample in (d) is shown inside circles which is a predominant place for a crack to  
585 initiate. The columnar grains run in and out of the images. Scale bars: 20 mm.

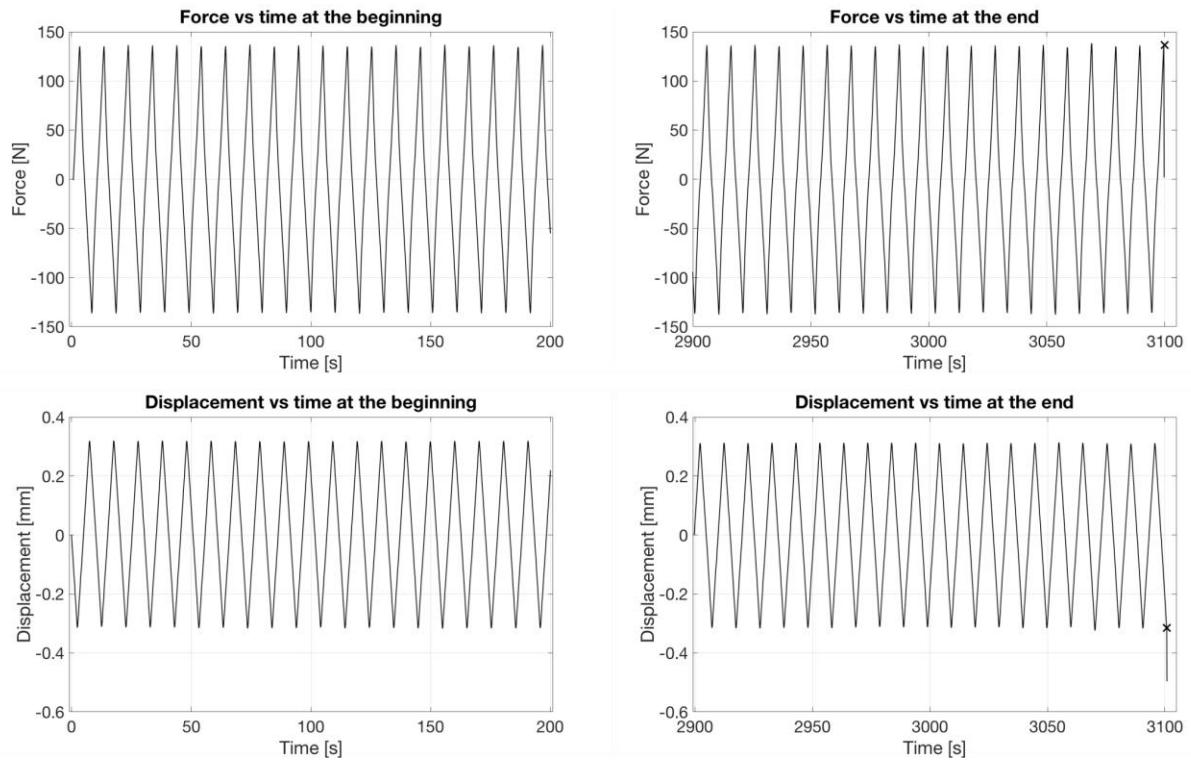


586  
587 **Figure 4.** Photograph of a sample from the bottom of an ice block of higher salinity ( $5.9\pm 0.6$  ppt) before cycling (a) and  
588 after (b) failure. Note a crack that propagated along whitish features in the area in (a) depicted by the circle. Scale bars:  
589 20 mm.

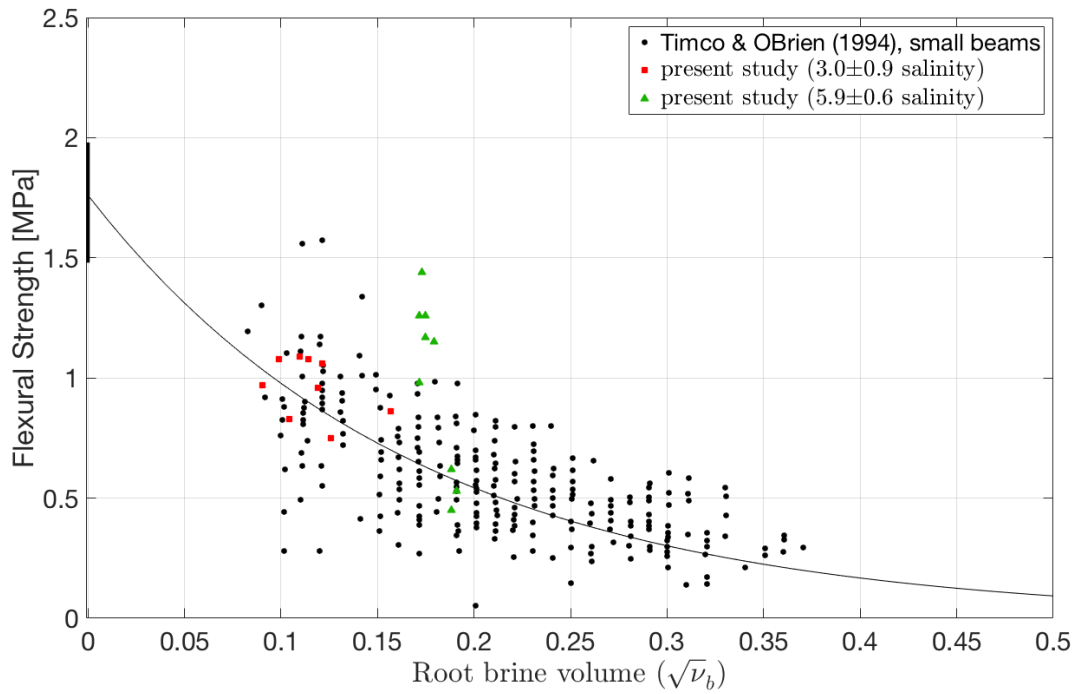


590  
591 **Figure 5.** Photograph (a) and sketch (b) of the four-point bending apparatus connected to an MTS hydraulic testing  
592 system (Iliescu et al., 2017; Murdza et al., 2020b). The upper part is attached to the frame of the machine while the mobile

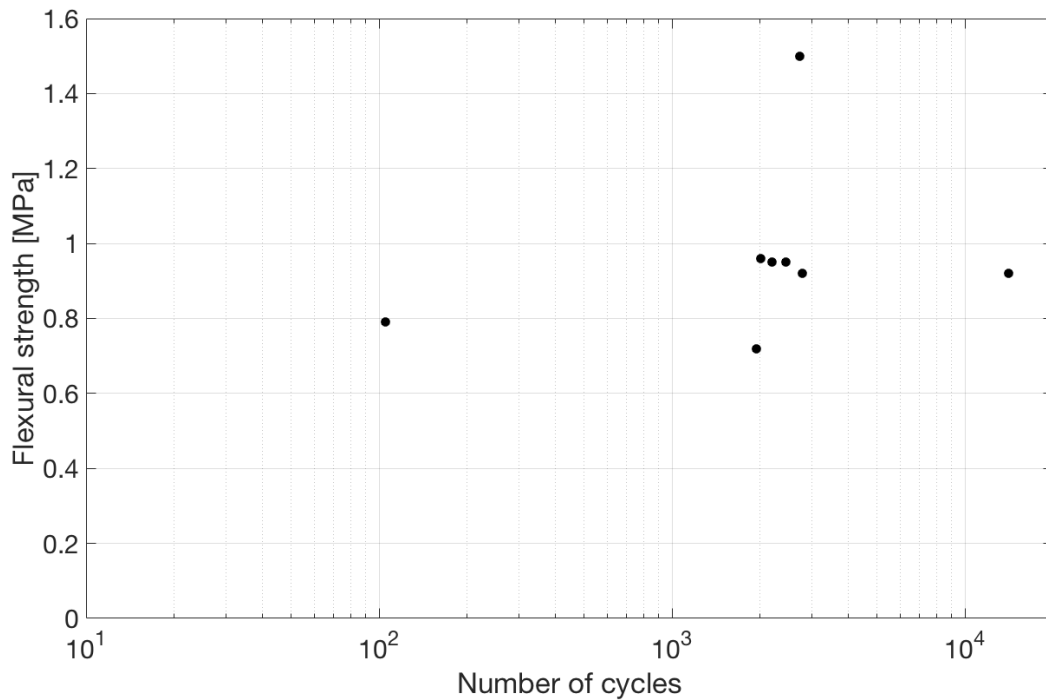
593 middle part is attached through a fatigue-rated load cell to the piston. The apparatus is made from an aluminum alloy;  
594 the loading cylinders are made from stainless steel.



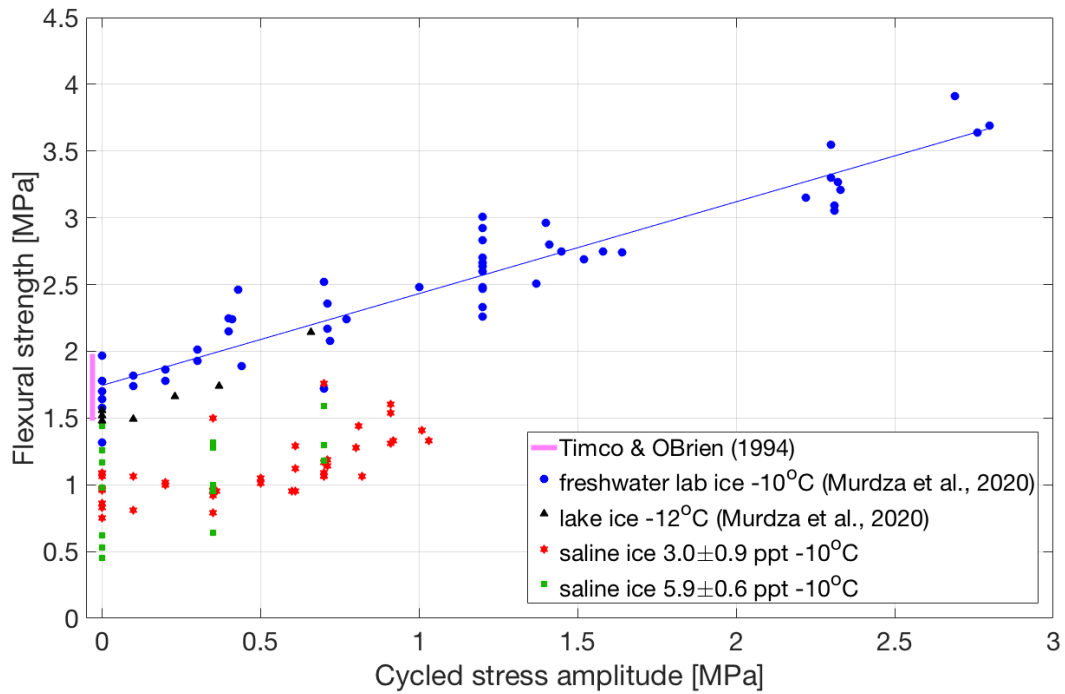
595  
596 **Figure 6. Curves of force/load and displacement vs. time for periods of 200 s near the beginning and near the end of**  
597 **cycling before fatigue failure occurred. Marker symbol “x” denotes a moment of specimen failure. Force of ~135 N**  
598 **corresponds to ~1.2 MPa.**



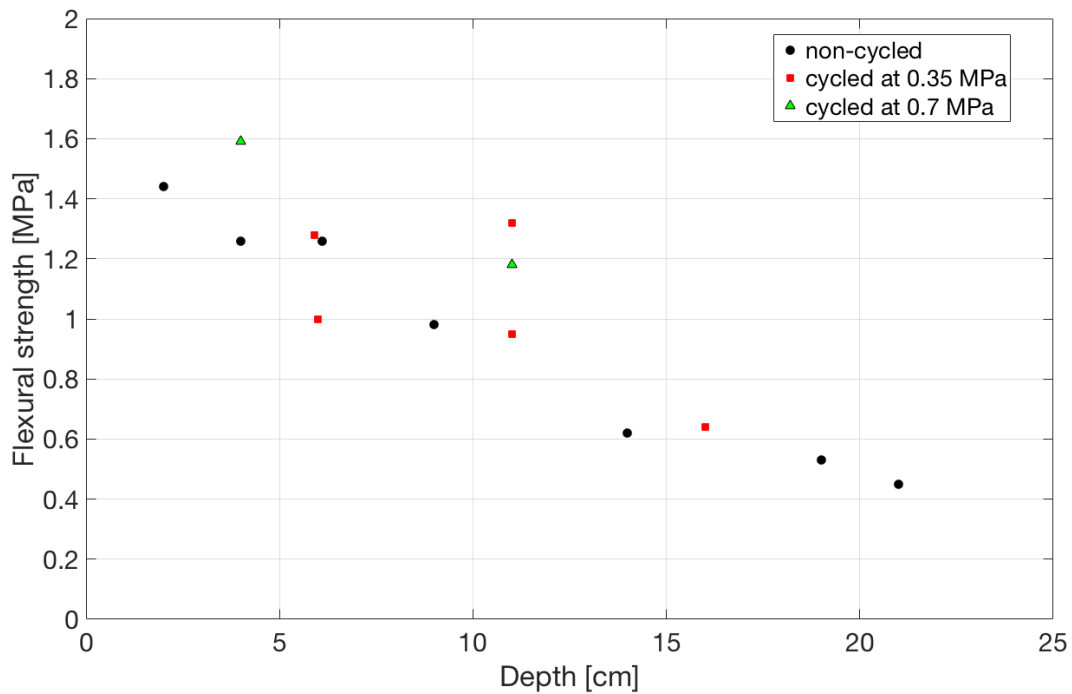
599  
600 **Figure 7. Flexural strength of saline ice as a function of root brine volume for the ice grown in the present study and for**  
601 **data from Timco and O'Brien (1994) for comparison.**



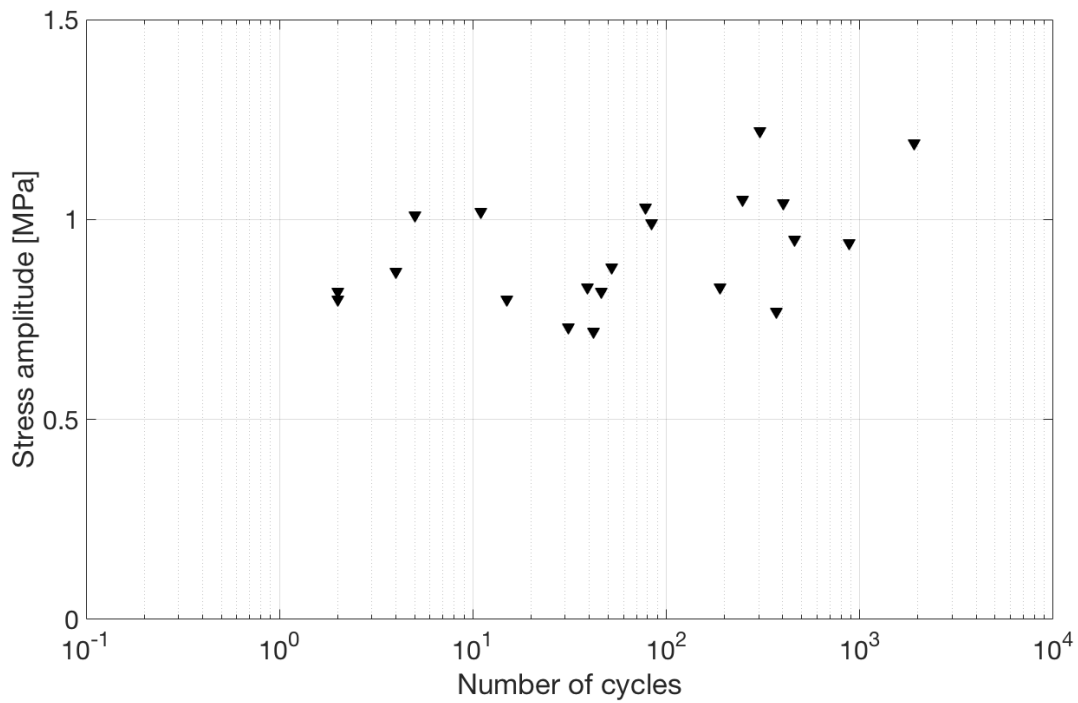
602  
603 **Figure 8. Flexural strength and the corresponding number of cycles imposed for saline ice of lower salinity (3.0±0.9) ppt**  
604 **cycled at 0.35 MPa outer-fiber stress amplitude at -10 °C and 0.1 mm s<sup>-1</sup> outer-fiber center-point displacement rate.**



605  
 606 **Figure 9. Flexural strength of freshwater ice and saline ice of lower ( $3.0\pm 0.9$  ppt) and of higher ( $5.9\pm 0.6$  ppt) salinity as a**  
 607 **function of reverse-cycled stress amplitude. Freshwater ice laboratory and lake data are taken from (Murda et al., 2020b,**  
 608 **2021). Red five-pointed stars and green squares represent tests performed on saline ice of lower and higher salinities,**  
 609 **respectively, at  $0.1\text{ mm s}^{-1}$  and  $-10^\circ\text{C}$ . During all depicted tests the ice did not fail during cycling and was broken by**  
 610 **applying one unidirectional displacement until failure occurred.**

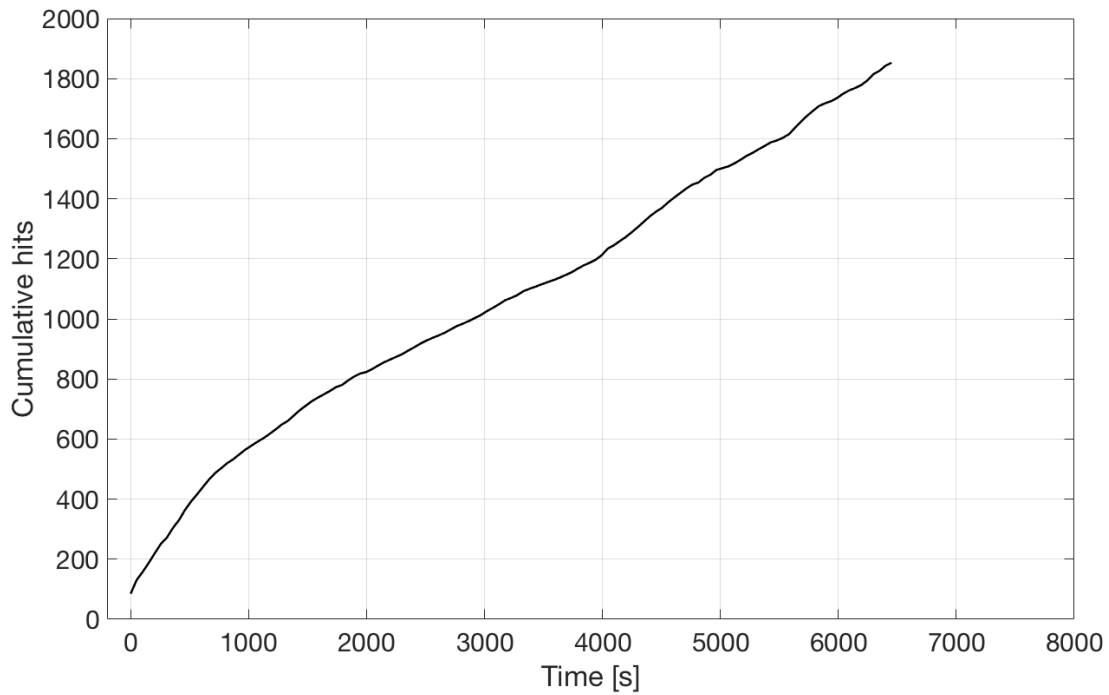


611  
 612 **Figure 10. Flexural strength as a function of position of saline ice samples of higher salinity ( $5.9\pm 0.6$  ppt) for different**  
 613 **cyclic amplitudes. The imposed number of cycles for specimens cycled at 0.35 and 0.7 MPa is  $\sim 2000$ .**

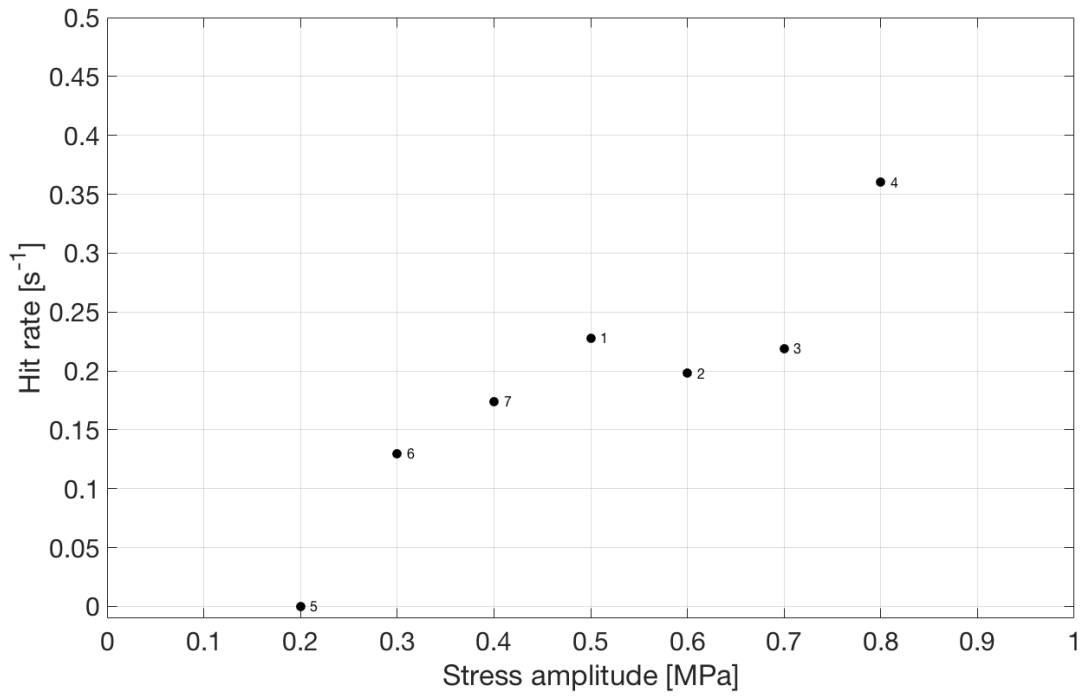


614  
 615 **Figure 11. Stress amplitude as a function of the number of cycles to fatigue fracture for saline ice of lower salinity**  
 616 **( $3.0 \pm 0.9$  ppt) tested at  $-10^\circ\text{C}$  and  $0.1 \text{ mm s}^{-1}$  outer-fiber center-point displacement rate.**

617



618  
 619 **Figure 12. Acoustic emissions (hits) against time for saline ice of lower salinity ( $3.0 \pm 0.9$  ppt), cycled at a stress amplitude**  
 620 **of  $0.5 \text{ MPa}$  at  $-10^\circ\text{C}$  at an outer-fiber displacement rate of  $0.1 \text{ mm s}^{-1}$ .**



621  
622 **Figure 13. Hit rate as a function of cycled stress amplitude for saline ice sample of lower salinity ( $3.0\pm 0.9$  ppt). Numbers**  
623 **show the order of cycling at different stress amplitudes.**

624  
625  
626